Crustal Structure and Evolution of the Arctic Caledonides: Results from Controlled-Source Seismology

Iselin Aarseth[a*], Rolf Mjelde[a], Asbjørn Johan Breivik[b], Alexander Minakov[b], Jan Inge Faleide[b], Ernst Flueh[c], Ritske S. Huismans[a],

[a] Department of Earth Science, University of Bergen, Allégaten 41, N-5007 Bergen, Norway

[b] Department of Geosciences, University of Oslo, P.O. box 1047, Blindern, N-0316 Oslo Norway

[c] GEOMAR, Wischhofstrasse 1-3, 24148 Kiel, Germany

[*] Corresponding author: E-mail address: iselin.aarseth@uib.no, Tel.: +47 45214608

Abstract

The continuation of the Caledonides into the Barents Sea has long been a subject of discussion, and two major orientations of the Caledonian deformation fronts have been suggested: NNW-SSE striking and NE-SW striking, respectively. A regional NW-SE oriented ocean bottom seismic profile across the western Barents Sea was acquired in 2014. In this paper we map the crust and upper mantle structure along this profile in order to discriminate between different interpretations of Caledonian structural trends and orientation of rift basins in the western Barents Sea. Modeling of P-wave travel times has been done using a ray-tracing method, and combined with gravity modeling. The results show high P-wave velocities (4 km/s) close to the seafloor, as well as localized sub-horizontal high velocity zones (6.0 km/s and 6.9 km/s) at shallow depths which are interpreted as magmatic sills. Refractions from the top of the crystalline basement together with reflections from the Moho give basement velocities from 6.0 km/s at the top to 6.7 km/s at the base of the crust. P-wave travel time modeling of the OBS profile indicate an eastwards increase in velocities from 6.4 km/s to 6.7 km/s at the base of the crystalline crust and the western part of the profile is characterized by a higher seismic reflectivity than the eastern part. This change in seismic character is consistent with observations from vintage reflection seismic data and is interpreted as a Caledonian suture extending through the Barents Sea, separating Barentsia and Baltica. Local deepening of Moho (from 27 km to 33 km depth) creates "root structures" that can be linked to the Caledonian compressional deformation or a suture zone imprinted in the lower crust. Our model supports a separate NE-SW Caledonian trend extending into the central Barents Sea, branching off from the northerly trending Svalbard Caledonides, implying the existence of Barentsia as an independent microcontinent between Laurentia and Baltica.

1. Introduction

The Barents Sea is located in the northwestern corner of the Eurasian continent (Fig. 1) where the assembly of the crystalline basement is related to the mid-Palaeozoic Caledonian orogeny (e.g. Roberts and Gee, 1985). Early post-Caledonian extension created Devonian basins on Svalbard, but it is unknown how this phase affected the offshore areas. Late Palaeozoic rifting in the Barents Sea formed basins that accumulated large amounts of evaporite deposits, whereas Mesozoic rifting events formed major Cretaceous basins followed by Cenozoic breakup and opening of the Northeast Atlantic (Roberts and Gee, 1985; Gabrielsen et al., 1990; Faleide at al., 2008; Gee et al., 2008; Smelror et al., 2009). It has long been recognized that Caledonian and older basement structures have influenced subsequent basin development and structural configuration in the Barents Sea (Harland and Gayer, 1972; Gabrielsen, 1984; Doré, 1991; Ritzmann and Faleide, 2007, Fig. 2). Due to petroleum exploration in the southwestern Barents Sea the structures of the main Mesozoic grabens, highs and platforms are fairly well known (e.g. Gabrielsen et al., 1990; Faleide et al., 1993; Breivik et al., 1998; Smelror et al., 2009; Henriksen et al., 2011a). The deep structure of the Late Palaeozoic basins and their relationship to the Caledonian orogeny still remains unclear in most of the western Barents Sea due to sparse distribution of wide-angle seismic data and poor resolution of multi-channel seismic (MCS) reflection data below the Permian sequence (Breivik et al., 2005). Ziegler (1988) proposed that the Scandinavian Caledonides extend northwestward linking up with the N-S trending Caledonides of Svalbard. Later interpretations involve two branches of the Caledonides, one through the eastern Barents Sea, and one through Spitsbergen (Gudlaugsson et al., 1998; Breivik et al., 2005; Henriksen et al., 2011a). Others consider only the eastern branch through the Barents Sea to be the suture (Doré, 1991; Harland et al., 1997; Gee et al., 2006, Fig. 2).

Further, it has been proposed that the Late Palaeozoic rifting in the southwestern Barents Sea developed in a north-easterly direction, following the inherited Caledonian structural grain, with a fan shaped distribution of rift basins and intra-basinal highs with orientations ranging from north-easterly in the main rift zone to northerly at the present continental margin in the west (e.g. Gudlaugsson et al., 1998; Breivik et al., 2005; Ritzmann and Faleide, 2007). However, based on new high quality aeromagnetic data covering the southwestern Barents Sea, Gernigon and Brönner (2012) and Gernigon et al. (2014) suggest that the sub-Permian basins and underlying basement grain have a dominantly NNW-SSE orientation and that Caledonian extensional collapse and subsequent rift evolution follow this trend. Contrary to previous interpretations the magnetic data do not recognize a NE-SW inherited Caledonian structural trend through the Barents Sea.

In areas where the deeper parts of the crust are difficult to image by conventional multi-channel seismic reflection data, wide-angle seismic experiments provide valuable information (e.g. Breivik et al., 2002). In 2014, three ocean bottom seismometer (OBS) profiles were acquired in the western Barents Sea (Minakov et al. (2014), Figs.1, 2), crossing the proposed trends of Caledonian structures and Late Palaeozoic rifts. The P-wave velocity- and gravity model along OBS Profile 2 are presented in this paper. The profile is 650 km long and has a NW-SE orientation, crossing the western Barents Sea from the Stappen High area north of Bjørnøya to the Nordkapp Basin. The primary objective of this paper is to investigate how pre-existing structures inherited from the Caledonian orogeny and subsequent Devonian extensional collapse in the western Barents Sea influenced subsequent Palaeozoic rift evolution.

2. Geological setting

Four major orogenic events have influenced the geology of the Barents Sea area: the Timanian (Ediacaran), Caledonian (Mid Silurian – Early Devonian) (Fig. 2), Uralian (Early Carboniferous – Late Permian/Triassic) and Eurekan orogens (Early Cenozoic). During the Timanian orogeny terranes accreted against the present-day northeastern margin of Baltica. The Timanian structural trend generally has a NW-SE orientation and extends into the South Barents Basin (Olovyanishnikov et al., 1997; Roberts and Siedlecka, 2002), but how far north and west these trends extend is uncertain. NW trending Timanian structures are exposed on the Varanger Peninsula in northernmost Norway (e.g. Roberts and Olovyanishnikov, 2004).

The Caledonian orogeny started in the Early Ordovician and culminated with the collision of Laurentia and Baltica in mid Silurian to Early Devonian time with the closure of the Iapetus Ocean (e.g. Gee et al., 2008). The Svalbard Archipelago comprises at least three crustal blocks and different hypotheses have been proposed for the Caledonian terrain assembly (Harland et al., 1997; Gee and Teben'kov, 2004; Cocks and Torsvik, 2011). The western terrains have Laurentian affinities (e.g. Harland et al., 1997), but the eastern part of Svalbard has been interpreted as an independent microcontinent between Laurentia and Baltica (Gudlaugsson et al., 1998; Torsvik et al., 2001; Breivik et al., 2002). The Uralian orogeny affected mostly the Eastern Barents Sea region during the collision between Laurussia (Laurentia and Baltica) and Siberia, with the closure of the Uralian Ocean (Churkin et al., 1981). Early Eocene compression formed the western Spitsbergen fold-and-thrust belt (e.g. Leever et al., 2011) during the Eurekan orogeny.

The complex structural framework of the Barents Shelf basement is a result of these collisional events. The Caledonian orogeny was followed by extensional collapse and Devonian graben formation. Post-orogenic sediments were deposited during the late Silurian-Devonian and compressively deformed in the Late Devonian tectonic phase referred to as the Svalbardian or Ellesmerian Event (Gee et al., 2008; Bergh et al., 2011; Blinova et al., 2013). Devonian rocks have mainly been preserved in north-south trending graben structures in Spitsbergen. Carboniferous rifting resulted in formation of several basins (e.g. Nordkapp Basin, Bjørnøya Basin, Tromsø Basin, Tiddlybanken Basin, Fig. 1) that collected large volumes of evaporites during the Late Carboniferous and Early Permian (Faleide et al., 1984; Gudlaugsson et al., 1998). Regional subsidence was established by the Early Permian and continued into the Triassic with deposition of clastic marine sediments. Rifting in the Middle Jurassic to Early Cretaceous created deep sedimentary basins and was followed by Early Cenozoic margin formation, opening of the Norwegian – Greenland Sea and the onset of seafloor spreading (Faleide et al., 1993). Early Cretaceous magmatism has affected areas northeast (e.g. Minakov et al., 2012) and south of Svalbard (Grogan et al., 2000; Breivik et al. 2005; Polteau et al., 2016) forming parts of the High Arctic Large Igneous Province (HALIP).

From mid-Miocene time to the present, the western Barents Sea has been regionally uplifted and eroded (Dengo and Røssland, 1992; Dimakis et al., 1998; Ohm et al., 2008; Henriksen et al., 2011b). Between 1500 m and 3200 m of the sedimentary sequence have been removed in our study area, leaving Triassic rocks close to the seafloor across the Bjarmeland Platform (Gudlaugsson et al., 1987) and only minor occurrences of Cretaceous sequences e.g. in the Nordkapp Basin (Faleide et al., 1984). The present western Barents Sea is dominated by a complex system of grabens and half-grabens, while the eastern Barents Sea consists of a single,

much larger N-S trending sag basin. This structural difference implies that the eastern and the western Barents Sea are underlain by different basement domains and structural grains, and there could also be variations in tectono-magmatic and metamorphic processes from west to east (e.g. Gac et al., 2012).

3. Data and methods

3.1. Data acquisition

OBS data were acquired using the research vessel Håkon Mosby during the summer of 2014 by the University of Bergen (UoB) in cooperation with the University of Oslo (UoO) and GEOMAR. These comprise two regional profiles in the western Barents Sea and a shorter profile in Storfjorden south of Svalbard. Gravity-, magnetic-, and bathymetry data were recorded continuously along the profiles using a LaCoste-Romberg shipboard gravity meter, a marine proton magnetometer and an echo sounder, respectively. Additionally, single-channel streamer data were acquired during seismic shooting. Four equal-sized air-guns with a total volume of 78.66 l (4800 in^3) were fired every 200 m (approx. 80 s) along each profile. The data were recorded by digital GEOMAR Ocean Bottom Seismometers recording both P-wave (vertical geophone and hydrophone) and S-waves (two orthogonal horizontal geophones). Navigation is based on the Differential Global Positioning System (DGPS). Profile 2 was shot in two segments where the instruments were redeployed from one segment to the other, each containing 20 OBSs deployed at a typical distance of 15-20 km, with 3 OBSs overlapping between the segments. Each segment gave a seismic record 394.6 km (NE) and 395.4 km (SE) long, respectively. With an overlap of 128.7 km the total length of the profile is 661.3 km.

3.2. Data processing

Preprocessing of the seismic data was done at GEOMAR, including cutting raw data into traces of 60 s, adjusting for instrumental clock drift, tieing to navigation, trace normalization and conversion to SEG-Y format. The OBS positions were then corrected for physical instrument drift. Further processing was done at UiB/UiO, including band pass filtering (4-16 Hz), spiking deconvolution (to compress the wavelet and suppress ringing) and automatic gain control (1 s window) to boost the far-offset signals. A reduction velocity of 8 km/s was applied in order to compress the time scale and obtain nearly horizontal refractions from the upper mantle. Processing of gravity data was done at UiO and included correction of relative gravity meters readings using measurements at reference points in Tromsø and Longyearbyen, subtraction of normal gravity field computed for the WGS84 model, and Eötvös correction. The instrument drift was checked by gravity measurements in the port in Tromsø before departure and upon arrival using marine- and land gravimeters, and the drift was within 1mGal. A Butterworth low-pass filter with cutoff wavelength of 5 km and the order of eight was applied to the gravity data. Comparison of the obtained free-air gravity anomaly with a regional dataset (ArcGP grid, Kenyon et al., 2008) shows a good match, however our measurements have a significantly better resolution.

3.3. Travel time modeling using Rayinvr

In order to map the crustal and upper mantle structure along the profile, a P-wave velocity model has been created using travel times recorded on the OBS hydrophone and vertical geophone components. The modeling was done using Rayinvr, a ray-tracing forward/inversion software

developed by Zelt and Smith (1992). It allows an iterative approach based on trial and error until a reasonable fit between interpreted and calculated travel time curves is achieved. Following the forward modeling, inversion is performed layer by layer separately on velocity- and depth nodes. The inversion is useful for finding solutions in areas with complex geology and to derive resolution statistics.

Velocity models based exclusively on travel times recorded on widely spaced OBSs are non-unique and dependent on ray coverage, but additional constraints can be obtained from including other types of data. Information from MCS data and gravity data has thus been included to supplement the velocity model. The OBS profile is shot along an existing MCS profile, IKU-H (Fig. 1), and published interpretations of this line from Gudlaugsson et al. (1987) and Ritzmann and Faleide (2007) (Fig. 12) was used in the initial model building. Water depths were taken from the echo sounder data and the water layer was given a velocity of 1.48 km/s, a typical velocity for arctic seas (Grad et al., 2011). The geometry and velocity of the water layer was fixed during the modeling. A top-down strategy was used, starting with arrivals from the sedimentary section. The Rayinvr code allows for ray tracing of refracted-, reflected- and head waves. The goal is to obtain a velocity model that minimizes the travel time residuals (difference between picked and calculated arrivals) and where rays can be traced for as many picks as possible (Zelt and Forsyth, 1994). Arrivals on each of the individual OBS records are interpreted and used in the modeling. Data and model examples are show in Figs. 3-7, OBS 229, 226, 224, 214 and 212 are chosen because these records generally have a good data quality and illustrates the main features of the velocity model. Phase names used in the figures are listed in Table 1. During the interpretation each pick is given an uncertainty in time, often assigned to ± one typical cycle width of the phase (Breivik et al., 2003), and the goodness of fit can be estimated using a

chi-squared (χ^2) criterion (e.g. Zelt and Forsyth, 1994). Typical uncertainties for the best arrivals are estimated to ±50 ms. Most Moho arrivals are given an uncertainty of ±90 ms if they are strong and clear, larger if they are weak. During the modeling an effort was made to obtain a χ^2 value of 1, which means that the travel time residual is equal to the pick uncertainty. A lower χ^2 value indicates overfitting (travel time residuals are less that the uncertainty of the picks), while a value larger than 1 imply that the residuals are higher that the pick uncertainty.

4. Results

4.1. P-wave travel time modeling

The final P-wave velocity model is divided into thirteen layers (Fig. 8). Some layers have similar velocities, but different velocity gradient. The quality of the data is generally good, however OBS 201, 221, 232 and 236 did not provide any useful data. The hydrophone component gave the best data for most of the stations, but on seven stations the vertical geophone component provided better data. The water layer (layer 1) is modeled with a constant velocity of 1.48 km/s and the water depth varies between 40 and 400 m along the profile. The youngest sedimentary rocks (layer 2), identified from MCS data tied to nearby wells, are Cretaceous in age (e.g. Faleide et al., 1984). Layer 2 has an average velocity of about 3.5 km/s and is thickest (1500 m) in the southeastern part of the profile within the Nordkapp Basin, and pinches out towards the northwest. In the NW end of the profile the velocities are higher, around 4.0 km/s just below the seafloor (layer 3). Based in interpretations of IKU-H (Gudlaugsson et al., 1987) the age of this sequence is expected to be Triassic.

A high-velocity layer is observed at a depth of 2 km on OBS 223-227 (layer 4). A velocity of 6 km/s gives a good fit between observed and calculated travel time however, shallow high velocities made it difficult to trace rays in the sedimentary section beneath layer 4. The velocity was therefore reduced from 6.0 km/s to 5.7-5.8 km/s, which gives a poorer fit but more rays in the deeper layers. Layer 4 is approximately 200 m thick and 80 km long. Early Cretaceous magmatism has previously been reported in the area (Grogan et al., 2000; Breivik et al., 2002, 2003; Polteau et al., 2016) and the shallow high velocity layer is interpreted as a magmatic sill. Refractions from layer 6 require quite high velocities (5.8-5.9 km/s) Modeling of OBS 223 and 224 (Fig. 5) indicate velocity inversions in the sedimentary section and a low velocity layer (layer 5) had to be introduced beneath the sill in order to model refractions in layer 6. Layer 6 has lateral velocity variations that may represent change in lithology.

OBS 202, 203 and 204 are located in the Nordkapp Basin where salt diapirs (layer 7) rise to the seabed. At OBS 203 and 204 high-velocity arrivals are observed close to the seabed. MCS data (Grimstad, 2016) were used to constrain the geometry of the salt and the sedimentary layering in the Nordkapp Basin, and two strong reflections were interpreted as near Base Cretaceous Unconformity (BCU) and near Top Permian, respectively. The modeling is very sensitive to geometry, and the steep flanks of the salt make it difficult to trace rays through it. No refractions have been modelled in the salt; however several Moho reflections pass through it e.g. on OBS 212 (Fig. 7). Based on these arrivals the salt diapirs were modeled with a velocity of 5.0 km/s. Due to complex geometry and limited data quality no rays where traced at all for OBS 202 and 203. Velocity measurements from the sedimentary section just above top basement (layer 8) show a velocity of 5.8 – 5.9 km/s. A low contrast in seismic impedance between the sedimentary section and top of the crystalline basement results in weak or absent arrivals from this interface,

making the interpretation uncertain. Some good basement refractions (P_g) have been recorded, mainly on OBS 214, 215, 218, 220, 226 and 227, constraining the velocity at top basement in the middle of the profile to 6.2 km/s. OBS 226 (Fig. 4) shows one of the strongest top basement arrivals as a refraction for larger offsets and a reflection for shorter offsets. OBS 226 also has some strong reflections from within the crystalline crust. Top basement is shallowest in the central parts of the model (7-8 km) and deepens to about 10 km beneath the Sørkapp Basin in the NW, and 12 km Nordkapp Basin in the SE (Fig.8). Primarily based on the move-out of Moho reflections a velocity of 6.4-6.5 km/s has been modeled at base of the crust in the western part of the profile, while it increases to 6.7 km/s and 6.6 km/s in central and eastern parts, respectively. Many intra crustal reflections, sometimes of high amplitude, were identified. These events seem to originate from two levels, and the basement has therefore been divided into three layers (layer 9, 11 and 12). Several reflective events did not fit this layering and floating reflectors were therefore introduced. Layer 10 is a high velocity (6.9 km/s) layer at a depth of about 11 km. It has a limited extent and can only be seen on OBS 214 (Fig. 6). It may be interpreted as an intra-crustal sill intrusion.

OBS 229 offers a lot of information at offsets up to 190 km (Fig. 3). Clear refractions give velocities of 5.8-5.9 km/s in the sedimentary sequence (layer 6). The record shows a very strong Moho reflection and the move-out of this event is used to constrain the average velocity in the crust. A weak refraction from the upper mantle (P_n) is also recorded. Below the Moho there are some relatively strong reflections (P_FP) that seems to originate from within the top 10-15 km of the mantle. This upper mantle reflectivity seem to dip to the west-northwest, however they are not constrained by reversed observations and could have other origins.

Between 260 km and 300 km in the model (Fig. 8) Moho deepens by 6 km (from 27 km to 33 km) over a distance of 40 km. This is recorded particularly well on OBS 224 (Fig. 5), where the P_MP phase is recorded at about 6 s (reduced travel time) on the left side and about 7 s (reduced travel time) on the right side. Around 310 km (model distance) the Moho shallows to 28 km creating a "root structure" in the lower crust. This feature has been recorded consistently on neighboring OBSs. Another increase in Moho depth is observed on OBS 214 (Fig. 6) at 400 km along the profile. OBS 212 (Fig. 7) shows strong Moho reflections and a weak P_n phase, but there is limited information from within the crystalline crust. Some intra crustal reflections do appear when filtering away the highest frequencies. Refractions from the upper mantle (layer 13) recorded on OBS 211, 212, 214, 218, 220 and 223 fit well with a velocity of 8.0 km/s in the upper mantle.

4.2. Velocity model assessment

An assessment of the velocity model is done in order to evaluate how well the different parts of the model are constrained. The normalized $\chi^2$and RMS travel time residuals for the modeled phases are presented in Table 2, and ray hits for the final velocity model are shown in Fig. 9a. Most of the phases have a χ^2 value close to 1. Generally, ray coverage is best in the central parts of the profile, and the model is best constrained between 100 km and 530 km. Ray coverage is limited at both ends of the profile making these areas poorly resolved. Sedimentary layers 2, 3 and 6 is well covered with refracted waves and the velocity here are fairly well constrained. The shallow sill intrusion (layer 4) is not covered by many rays, but clear head waves have been modeled from this layer on OBS 229 and OBS 227-223. Clear refractions in the NW constrain

the velocity at the top of layer 8, but the velocity structure is not well resolved in the SE part of the model.

The inversion tool in Rayinvr is used to obtain a resolution matrix in order to estimate how well the individual velocity nodes are constrained (Fig. 9b). Velocity nodes were inverted layer by layer (node spacing 15-50 km), while keeping the geometry fixed, using only refracted arrivals. Values range from 0 to 1, with values from 0.5 and up indicating a fairly well resolved parameter (Zelt and Smith, 1992). The depth node resolution was estimated for Moho (node spacing 10-30 km), while keeping the velocity fixed using both reflections and refractions. Larger circles around the depth nodes in Fig. 9b indicate better resolution.

The top of the crystalline crust is best constrained in the central parts of the model. In the NW end of the profile no top basement refractions have been recorded and the interpretation is based on reflections only. No direct velocity control was obtained from within the lower crust (layer 11 and 12); however the move-out of clear Moho reflections, recorded on almost all stations, gives the average velocity in the crust throughout the model, with the apparent velocity at maximum offset (50-200 km) approaching the velocity in the lowermost crust. Moho is constrained by both reflected and refracted arrivals. However, the poor control on velocity structure in the lower crust makes the Moho depth somewhat uncertain, particularly in the southern 100 km of the model. Fig 9b indicates a poor depth node resolution in the crustal root area. The ray hit is limited due to the complex geometry, however clear PmP arrivals from OBS 226-223 and OBS 218 have been modelled here, suggesting that this feature is real. Some refractions from the upper mantle have been modeled, but the velocity structure here is not well constrained.

4.3. Gravity modeling

The ray-coverage (Fig.9a) is controlled by the acquisition geometry and P-wave velocities. Gravity data have a different sampling and have the potential to add information to the model. A two-dimensional gravity model was made along the profile using the Oasis montaj GM-SYS Profile Modeling software. The gravity profile used in the modeling was recorded together with the OBS data and the observed gravity anomalies vary between -56 and 56 mGal. The strong positive gravity anomaly observed at the NW end of the profile is associated with the continent-ocean transition (COT) located a few km west of our profile, and has also been modelled by Breivik et al. (2003). There is also a positive gravity anomaly over the Gardarbanken High and a negative gravity anomaly due to the salt diapirs in the Nordkapp Basin. The velocity model was converted to a gravity model keeping the geometry of the layers. The average velocity in each layer was used to estimate initial density from an empirical velocity-density relationship (Ludwig et al., 1970; Barton, 1986). The model was extended 30 000 km in each direction to avoid edge effects. The results of the gravity modeling are presented in Fig. 10. The sedimentary section has been divided into three layers with densities of 2400 kg/m^3, 2620 kg/m^3 and 2740 kg/m^3. Additionally, the zone of increased velocities (part of layer 6, Fig.8) above Gardarbanken High were modeled with a density of 2700 kg/m^3. Consistent with the velocity model, the crystalline crust have been divided into an upper, middle and lower layer and given densities based on the average velocity in each block, with values ranging from 2800 kg/m^3 to 2910 kg/m^3. These values are comparable to other models in the area, e.g. Marello et al. (2010) who used densities from 2710-2780 kg/m^3 and 2940 kg/m^3 for the upper and lower crust, respectively, and Klitzke et al. (2016) who used 2660-2800 kg/m^3 and 2977-3025 kg/m^3 for the upper and lower crust, respectively. The lateral increase in velocity eastwards is modelled as increased densities,

dividing the crust into blocks. The data from Ludwig et al. (1970) show a considerable scatter in the velocity-density relationship, and a variation of ±200 kg/m^3 is possible. During the modeling, the initial densities were not adjusted more than ±30 kg/m^3. The lithosphere-asthenosphere boundary (LAB) is based surface wave tomography for the Barents Sea (Levshin et al., 2007) as applied by Klitzke et al. (2016). In accordance with the recent model of Klitzke et al. (2016), densities of 3330 and 3180 kg/m^3 have been used for the upper mantle lithosphere and asthenosphere, respectively.

Dividing the crust into even more block or adjusting the initial densities more gave a slightly better fit with the observed gravity field. However, in order to keep the model as simple as possible and without too many modifications, an error of 5.416 mGal is considered an acceptable fit between the observed and calculated gravity field. An attempt was also made to adjust the LAB, while keeping the crust homogenous, but this resulted in a very unrealistic topography of the LAB. The source of the anomaly above Gardarbanken High can lie in the sedimentary section or the crystalline crust (or both). The observed gravity can also be reproduced by introducing a block of increased density (3370 kg/m^3) in the upper mantle.

5. Discussion

5.1. Crustal structure

Velocities just below the seafloor vary from 3.4 km/s in the southeast to 4.0 km/s in the northwest. High velocities in the shallow sedimentary section are attributed to Late Cenozoic uplift and erosion (Eidvin et al., 1993; Dimakis et al., 1998; Grogan et al., 1999; Ohm et al., 2008; Henriksen et al., 2011b). Erosion has removed up to 3200 m from the sedimentary section in the northwestern end of the profile and about 1600 m in the southeastern end (e.g. Dimakis et

al., 1998; Henriksen et al., 2011b). Increased velocities in the northwest end of the profile correlate with increased net erosion in the Stappen High area. The deepest basement can be found under the Sørkapp- and Nordkapp Basins (Fig. 8) where the depths reach 10 and 12 km, respectively. The Sørkapp Basin is defined at Permian and Triassic levels (Gabrielsen et al., 1990; Grogan et al., 1999) (Fig.1). The main basin subsidence occurred in the Triassic, but reflection seismic data indicate that Palaeozoic carbonates is underlain by an older basin, possibly of Early Carboniferous and/or Devonian age (Gabrielsen et al., 1990). Gudlaugsson and Faleide (1994) and Breivik et al. (2003, 2005) identified a deep basin a few km northeast of our profile with basement depths reaching 14 km, coinciding with the Sørkapp Basin. This basin was constrained to the west and north, but not to the east and south. The basin modeled here could be the southwest continuation of that basin, were the southeastern flank is constrained by top basement refractions and the northwestern flank by top basement reflections on OBS 234 and IKU-H. The basin coincides well with the model of Klitzke at el. (2016), who also modeled basement depth around 10 km in this area. The Sørkapp Basin is often drawn as a slightly N-S elongated basin on structural maps (e.g. Gabrielsen et al., 1990; Faleide et al., 1993) however, Anell et al. (2014) suggested a NE-SW to E-W trend. Comparing our model with three older OBS profiles modeled by Breivik et al. (2002, 2005) (Figures 1 and 11) we favor a NE-SW trend of the Sørkapp Basin, in accordance with previous interpretations of rift basins in southwestern Barents Sea (e.g. Gudlaugsson et al., 1998; Faleide et al., 2008). The outline of the Sørkapp Basin is drawn on Fig. 11. Its northwestern and southeastern boundary is fairly well constrained by OBS data, whereas the continuation to the east and southwest is uncertain.

The modeled profile is shot along the deep seismic line IKU-H, and layer boundaries from the time-converted velocity model are overlain on interpretations of IKU-H in Fig. 12. There is a

good fit between the OBS data and the MCS data in the sedimentary section (at 1.9 s) in the NW end of the profile, but the two datasets seem to have picked up slightly different reflections across the Bjarmeland Platform. Top of the crystalline crust is difficult to interpret from MCS data, especially in the eastern part. In the NW end the top of the chaotic reflective zone around 3 s could be interpreted as top of the crystalline crust, but from the OBS data it is interpreted to lie deeper under the Sørkapp Basin. Assuming the P-wave velocity model from the OBS data is correct, the top of the chaotic reflective package could be interpreted as meta- sedimentary rocks overlying crystalline crust.

The Moho topography between 260 km and 340 km in the model is interpreted as a Caledonian "root structure". Similar structures associated with high velocities in the upper mantle (8.5 km/s) have been modeled in the Sentralbanken High region (Breivik et al., 2002) where high velocities and densities in the upper mantle were interpreted as eclogitized oceanic crust associated with a proto-Caledonian subduction zone, with the crustal root as a remnant of the continental collision. A crustal root structure has also been observed along the deep seismic line IKU-D (Fig. 1) south of Svalbard, and interpreted to be a proto-Caledonian subduction zone dipping to the west (Gudlaugsson and Faleide, 1994; Breivik et al., 2005). Farther southeast along the profile, around 400 km, another prominent increase in Moho depth has been modeled. This structure is most likely related to the boundary between two different basement domains (Figs. 12 and 13), but how it is linked to structures shallower in the crust is uncertain. There is generally a good correspondence in Moho depth between OBS data and IKU-H. In the western part of IKU-H the basement is very reflective down to about 10 s and the base of this reflective zone is interpreted as Moho. In the velocity model Moho is located 0.5-1.0 s shallower, but many floating reflectors have been modeled in the upper mantle, suggesting that the base of the reflective zone on IKU-H

does not represent Moho, but rather a reflective zone in the upper mantle. Another explanation for the misfit could be that OBS data generally measure more horizontal and therefore higher velocities, resulting in a shallower Moho interpretation. Additionally, some of the dipping reflections on IKU-H could be diffractions (the line is not migrated, but a dip filter have been applied to remove some of the diffractions). On OBS 229 a weak arrival with an apparent P-wave velocity of 7.1 km/s has been modelled as a Pn phase. A good fit between observed and modelled travel times can be achieved by introducing as a high-velocity (7.1 km/s) layer in the lower crust. However, such a layer disrupts several strong PmP arrivals on OBS 223-229. Lacking support from other OBSs, it was considered more important to fit the strong PmP-arrivals, and a high-velocity layer in the lower crust was not included in the model.

5.2. Tectonic domains and comparison with nearby seismic profiles

The modeled profile crosses three older OBS profiles and velocities and densities at the cross points are listed in Table 3. In cross point 1 (profile 3e from Breivik et al. (2003) and OBS 236, Fig. 1), the depth to crystalline crust is 8 km in both profiles. Cross point 2 and 3 is located in the central parts of the model (at OBS 224 and 229, respectively) and at the southern ends of Profile 1 and 2 from Breivik et al. (2005). The difference in modelled depth to crystalline crust is quite large at the cross points, between 3-4 km. However, the southern ends of Profile 1 and 2 is poorly constrained by seismic data and the basement depths are uncertain, and the interpretation from our study is therefore preferred. Breivik et al. (2003) has modeled a deeper Moho (29 km) compared to this study (26 km). A northwestward shallowing of the Moho was introduced in cross point 1 based on the positive gravity anomaly at the NW end and the COB located a few km west of the profile. This shallowing of Moho was also modelled by Breivik et al. (2003). Cross

point 1 is at the northwestern edge of the model and is poorly constrained by seismic data, and no thermal effects of the adjacent young oceanic lithosphere were incorporated, so the old model should be the most reliable in this area.

The velocity model in Fig. 8 shows significantly lower basement velocities in the western (6.05-6.5 km/s) than the eastern part (6.2-6.7 km/s). This eastwards increase in velocity was also modelled by Breivik et al. (2003) farther north and could to be related to a possible suture between Laurentia in the west and Barentsia in the east (Figs. 11 and 13). Based on the velocity structure in the crystalline crust and the geometry of the upper mantle reflectivity (Fig. 8) our model supports the interpretation of Breivik et al. (2003) with a westward dipping suture between Laurentia and Barentsia. However, we propose that the Laurentia-Barentia suture is located about 50 km farther west than the suture proposed by Breivik et al. (2003), cutting top basement close to the location of OBS 228 (Fig. 11, 13). Primarily based on potential field data this suture has been traced northwards in Storfjorden and along the Billefjorden Fault Zone. This is supported by Agard et al (2005) who documents a Caledonian subduction in western Spitsbergen and Krysinski et al. (2013) who modeled OBS profiles across Spitsbergen and Storfjorden (Fig. 11) and interpreted variations in crustal thickness, velocities and densities to represent the main Caledonian suture between Laurentia and Barentsia. The suture may also be traced further south, between the Bjørnøya Basin and the Loppa High (Clark et al., 2013, Fig. 11). No lateral velocity change can be observed across the Barentsia-Baltica suture from the modeled OBS data. However, the change in reflective character across this boundary, observed both from the OBS data (Fig. 9a) and vintage MCS data (Fig. 12), suggest that these two blocks consist of materials with different physical properties. An eastward decrease in reflectivity has also been observed further north along IKU-D, and has been proposed to represent a Caledonian suture zone

separating Barentsia from Baltica (Gudlaugsson and Faleide, 1994). This interpretation is supported by modeled OBS data along the same line (profile 3e, Fig. 1) (Breivik et al., 2003).

5.3. Tectonic model

Generally N-striking Caledonian basement with Laurentian affinities is exposed in the Svalbard Archipelago (Harland et al., 1997) and most of Svalbard's Caledonian terranes are considered to be the direct northerly continuation of the Caledonides of eastern Greenland (e.g. Higgins and Leslie, 2000). Caledonian migmatization is found as far east as Kvitøya (Gee 2004) (Fig. 2), about 100 km east of Nordaustlandet, suggesting that a substantial part of the Barents Shelf is underlain by Caledonian basement and that Caledonian suture(s) must be located even farther to the east. Deep drilling on Franz Josef Land reached turbidites of Vendian age with folding proposed to be Caledonian (Dibner, 1998). Farther northeast, on Severnaya Zemlya, folding and thrusting of Devonian Old Red Sandstone has been related to late Caledonian deformation (Lorenz et al., 2007). No Caledonian deformation has been recorded in the island of Novaya Zemlya. A Caledonian suture through the Barents Sea between Kvitøya and western Franz Josef Land has been favored (Gee et al., 2006; Barrère et al., 2011). The Caledonian deformation front has been inferred to trend northeastwards between Franz Josef Land and Novaya Zemlya (Fig. 2).

Based on the orientation of basins and highs on the Barents Sea shelf (e.g. Nordkapp Basin, Hammerfest Basin, Loppa High, and Sentralbanken High) it has been proposed that the Caledonian suture follows this northeasterly trend in the Barents Sea (Doré, 1991; Gudlaugsson et al., 1998). Gudlaugsson et al. (1998) and Breivik et al. (2002) suggested that the Caledonian orogeny consists of two branches north of Norway, one along western Spitsbergen and one

northeast through the Barents Sea. Torsvik et al. (2001) proposed that Svalbard acted as an independent crustal block in the early Palaeozoic, and probably collided with NE Greenland in Late Ordovician times, and subsequently colliding with Baltica during the Mid-Late Silurian. The model of Breivik et al. (2002) is in accordance with this interpretation, with the microcontinent "Barentsia" (not corresponding entirely to the islands of Svalbard) between Laurentia and Baltica. This scenario has also been supported by magnetic data (Marello et al., 2013), as Barentsia is distinguished from the rest of the Barents Sea shelf by its low-magnetic properties and large crustal thickness. Marello et al. (2013) agreed with the proposed location of the Barentsia-Baltica suture (Breivik et al., 2002) and extended it further north- northeastwards to the western Franz Josef Land. Breivik et al. (2002) proposed a Caledonian suture located under and following the trend of the Sentralbanken High, and interpreted the thickest parts of the crust to be created by a subduction zone dipping to the southeast, terminating in continent-continent collision. The central parts of the modeled profile lie in the southwestward continuation of the proposed suture trend, and a suture dipping to the southeast fits well with the observed change in reflective character and the deepening of Moho around 400 km (Fig. 12).The polarity of the suture can be discussed. A zone of westward dipping reflectivity in the lower crust along IKU-H has been interpreted by Gudlaugsson et al. (1987) as overthrusting eastwards. However, this zone is located so far to the west that is might be associated with the Svalbard Caledonides. Also the image along IKU-H is blurred by a lot of diffraction hyperbolas dipping in both directions, and it is very difficult to distinguish dip directions of faults or sutures from diffractions. Based on potential field data Marello et al. (2013) supports the possible location of the inferred suture but suggested a dip towards the northeast.

6. Summary and conclusions

We present a P-wave velocity model across the Arctic Caledonian basement province based on modeling of travel times recorded on 32 ocean bottom seismometer stations along a ~660 km long profile in the western Barents Sea. The geometry of the shallow sedimentary section is constrained by seismic reflection profiles. P-wave velocities in the sedimentary unit are generally higher in the northwestern part of the profile (4.2 – 5.2 km/s) than in the eastern (3.2 – 4.5 km/s), attributed to increased erosion towards Svalbard and the continental margin. Two zones of anomalously high velocities in the upper crust (6.0 km/s and 6.9 km/s) have been interpreted as magmatic sills, probably emplaced during the Early Cretaceous. Depth to basement is constrained to 7 km in the middle of the profile, increasing to 10 km and 12 km beneath the Sørkapp Basin and Nordkapp Basin, respectively. Combining the profile modeled here with previously published velocity models along nearby OBS profiles, we favor a NE-SW trend of the Sørkapp Basin. Local deepening of Moho (from 27 km to 33 km depth) creates "root structures" that can be linked to the Caledonian compressional deformation or a suture zone imprinted in the crust. A sharp increase in velocities in the crystalline basement (from 6.0-6.4 km/s in the northwest to 6.1-6.6 km/s in the southeast) has been interpreted in terms of two distinct tectonic terranes: Laurentia and Barentsia. We further infer a westward subduction of Barentsia beneath Laurentia based on the pattern of seismic velocities and geometry of mid-crustal reflectors. The eastwards decrease in reflectivity observed along a vintage multichannel seismic line (IKU-H) is supported by the new OBS data, and interpreted to represent the suture between Barentsia and Baltica. Our model supports the existence of a separate NE-SW trending Caledonian branch extending into the Barents Sea, linking up with the northerly trending Svalbard Caledonides, with Barentsia as an independent microcontinent between Laurentia and Baltica.

7. Acknowledgements

This work was supported by the Research Council of Norway FRINATEK program through BarPz project 234153. We would like to thank all the participating institutions and the crew onboard R/V Håkon Mosby. Ole Meyer, Stig Monsen and Patrice Bretel from the University of Bergen and Alexey Shulgin and Nina Lebedeva-Ivanova from the University of Oslo and Ann-Marie Vølsch, Jasmin Møgeltønder and Kathrin M. Lieser from GEOMAR are thanked for their contribution during the OBS acquisition. We also thank Alexey Shulgin for pre-processing parts of the OBS data. A.J. Breivik, J.I. Faleide and A. Minakov acknowledge support from the Research Council of Norway through its Centres of Excellence funding scheme, project number 223272. The modeling was done using Rayinvr provided by Dr. C. Zelt (Rice University, Houston). GMT (Wessel and Smith, 1998) has been used to generate several of the maps in this paper.

8. References

Agard, P., Labrousse, L., Elvevold, S., Lepvrier, C., 2005. Discovery of Paleozoic Fe-Mg carpholite in Motalafjella, Svalbard Caledonides: A milestone for subduction-zone gradients. Geology 33 (10), 761-764 doi: 10.1130/G21693.1.

Anell, I., Braathen, A., Olaussen, S., 2014. Regional constraints of the Sørkapp Basin: A Carboniferous relic or a Cretaceous depression? Marine and Petroleum Geology 54, 123-138 doi: http://dx.doi.org/10.1016/j.marpetgeo.2014.02.023.

Barrère, C., Ebbing, J., Gernigon, L., 2011. 3-D density and magnetic crustal characterization of the southwestern Barents Shelf: implications for the offshore prolongation of the Norwegian Caledonides. Geophysical Journal International 184 (3), 1147-1166, doi: 10.1111/j.1365-246X.2010.04888.x.

Barton, P.J., 1986. The relationship between seismic velocity and density in the continental crust – a useful constraint? Geophys. J. R. Astron. Soc. 87, 195-208 doi: https://doi.org/10.1111/j.1365-246X.1986.tb04553.x.

Bergh, S.G., Maher, H.D.Jr., Braathen, A., 2011. Late Devonian transpressional tectonics in Spitsbergen, Svalbard, and implications for basement uplift of the Sørkapp-Hornsund High. Journal of the Geological Society, London 168, 441-456, doi: 10.1144/0016-76492010-046.

Blinova, M., Faleide, J.I., Gabrielsen, R.H., Mjelde, R., 2013. Analysis of structural trends of sub-sea-floor strata in the Isfjorden area of the West Spitsbergen Fold-and-Thrust Belt based on multichannel seismic data. Journal of the Geological Society, London 170, 657-668 doi: 10.1144/jgs2012-109.

Breivik, A.J., Faleide, J.I., Gudlaugsson, S.T., 1998. Southwestern Barents Sea margin: late Mesozoic sedimentary basins and crustal extension. Tectonophysics 293, 21-44 doi: http://dx.doi.org/10.1016/S0040-1951(98)00073-0.

Breivik, A.J., Mjelde, R., Grogan, P., Shimamura, H., Murai, Y., Nishimura, Y., Kuwano, A., 2002. A possible Caledonide arm through the Barents Sea imaged by OBS data. Tectonophysics 355, 67-97 doi: http://dx.doi.org/10.1016/S0040-1951(02)00135-X.

Breivik, A.J., Mjelde, R., Grogan, P., Shimamura, H., Murai, Y., Nishimura, Y., 2003. Crustal structure and transform margin development south of Svalbard based on ocean bottom seismometer data. Tectonophysics 369, 37-70 doi: http://dx.doi.org/10.1016/S0040-1951(03)00131-8.

Breivik, A.J., Mjelde, R., Grogan, P., Shimamura, H., Murai, Y., Nishimura, Y., 2005. Caledonide development offshore-onshore Svalbard based on ocean bottom seismometer, conventional seismic, and potential field data. Tectonophysics 401, 79-117 doi: http://dx.doi.org/10.1016/j.tecto.2005.03.009.

Breivik, A.J., Verhoef, J., Faleide, J.I., 1999. Effect of thermal contrasts on gravity modeling at passive margins: results from the western Barents Sea. J. Geophys. Res. 104 (B7), 15293-15311 doi: 10.1029/1998JB900022.

Churkin, M.Jr., Soleimani, G., Carter, C., Robinson, R., 1981. Geology of the Soviet Arctic: Kola Peninsula to Lena river. In: Nairn, A.E.M., Churkin, M.J., Stehli, F.G. (Eds.). The Ocean Basins and Margins, The Arctic Ocean 5, 331-375.

Clark, S.A., Faleide, J.I., Hauser, J., Ritzmann, O., Mjelde, R., Ebbing, J., Thybo, H., Flüh, E., 2013. Stochastic velocity inversion of seismic reflection/refraction traveltime data for rift structure of the southwest Barents Sea. Tectonophysics 593, 135-150 doi: http://dx.doi.org/10.1016/j.tecto.2013.02.033.

Cocks, L.R.M., Torsvik, T.H., 2011. The Palaeozoic geography of Laurentia and western Laurussia: A stable craton with mobile margins. Earth-Science Reviews 106 (1-2), 1-51 doi: http://dx.doi.org/10.1016/j.earscirev.2011.01.007.

Dengo, C.A., Røssland, K.G., 1992. Extensional tectonic history of the western Barents Sea. In: Larsen, R.M., Brekke, H., Larsen, B.T., Talleraas, E. (Eds.) Structural and tectonic modelling and its applications to petroleum geology. Norwegian Petroleum Society Special Publication, Trondheim 1, 91-107.

Dibner, V.D., 1998. The geology of Franz Joseph Land – an introduction. In: Solheim, A., Musatov, E., Heintz, N. (Eds.) Geological Aspects of Franz Joseph Land and the Northernmost Barents Sea. Norsk Polarinstitutt Meddelelser 151, 24-46.

Dimakis, P., Braathen, B.I., Faleide, J.I., Elverhøi, A., Gudlaugsson, S.T., 1998. Cenozoic erosion and the preglacial uplift of the Svalbard-Barents Sea region. Tectonophysics 300, 311-327 doi: http://dx.doi.org/10.1016/S0040-1951(98)00245-5.

Doré, A.G., 1991. The structural foundation and evolution of Mesozoic seaways between Europe and the Arctic. Palaeogeogr. Palaeoclimatol. Palaeoecol. 87, 441-492 doi: https://doi.org/10.1016/0031-0182(91)90144-G.

Eidvin, T., Jansen, E., Riis, F., 1993. Chronology of Tertiary fan deposits off the western Barents Sea: implications for the uplift and erosion history of the Barents shelf. Marine Geology 112, 109-131 doi: https://doi.org/10.1016/0025-3227(93)90164-Q.

Faleide, J.I., Gudlaugsson, S.T., Jacquart, G., 1984. Evolution of the western Barents Sea. Marine and Petroleum Geology 1, 123-150 doi: https://doi.org/10.1016/0264-8172(84)90082-5.

Faleide, J.I., Tsikalas, F., Breivik, A.J., Mjelde, R., Ritzmann, O., Engen, O., Wilson, J., Eldholm, O., 2008. Structure and evolution of the continental margin off Norway and Barents Sea. Episodes 31 (1), 82-91.

Faleide, J.I., Vågnes, E, Gudlaugsson, S.T., 1993. Late Mesozoic-Cenozoic evolution of the south-western Barents Sea in a regional rift-shear tectonic setting. Mar. Pet. Geol. 10, 186-214 doi: https://doi.org/10.1016/0264-8172(93)90104-Z.

Gabrielsen, R.H., 1984. Long-lived fault zones and their influence on the tectonic development of the southwestern Barents Sea. Journal of the Geological Society, London 141, 651-662 doi: 10.1144/gsjgs.141.4.0651.

Gabrielsen, R.H., Færseth, R.B., Jensen, L., Kalheim, J.E., Riis, F., 1990. Structural elements of the Norwegian continental shelf: Part 1. The Barents Sea Region. NDP Bull., vol. 6. Nor. Petrol. Dir., Stavanger, Norway.

Gac, S., Huismans, R.S., Podladchikov, Y.Y., Faleide, J.I., 2012. On the origin of the ultradeep East Barents Sea basin. Journal of Geophysical Research 117, B04401 doi:10.1029/2011JB008533.

Gee, D.G., 2004. The Barentsian Caledonides: death of the High Arctic Barents Craton. In: Smelror, M., Bugge, T. (Eds.) Arctic Geology, Hydrocarbon Resources and Environmental Challenges. NGF Abstracts and Proceedings 2, 48-49.

Gee, D.G., Bogolepova, O.K., Lorenz, H., 2006. The Timanide, Caledonide and Uralide orogens in the Eurasian high Arctic, and relationships to the palaeo-continents Laurentia, Baltica and Siberia. In: Gee, D.G., and Stephenson, R.A. (Eds.) European Lithosphere Dynamics. Memoirs Geological Society of London 32, 507-520.

Gee, D.G., Fossen, H., Henriksen, N., Higgins, A.K., 2008. From the Early Paleozoic platforms of Baltica and Laurentia to the Caledonide Orogen of Scandinavia and Greenland. Episodes 31 (1), 44-51.

Gee, D.G., Teben'kov, A.M., 2004. Svalbard: a fragment of the Laurentian margin. In: Gee, D.G., Pease, V.L. (Eds.) The Neoproterozoic Timanide Orogen of Eastern Baltica. Memoirs Geological Society of London 30, 191-206.

Gernigon, L., Brönner, M., 2012. Late Palaeozoic architecture and evolution of the southwestern Barents Sea: insights from a new generation of aeromagnetic data, J. Geol. Soc. London, 169 (4), 449-459 doi: 10.1144/0016-76492011-131.

Gernigon, L., Brönner, M., Roberts, D., Olesen, O., Nasuti, A., Yamasaki, T., 2014. Crustal and basin evolution of the southwestern Barents Sea: From Caledonain orogeny to continental breakup. Tectonics 33, 347-373 doi: 10.1002/2013TC003439.

Grad, M., Mjelde, R., Czuba, W., Guterch, A., Schweitzer, J. and the IPY Project Group. 2011. Modelling of seafloor multiples observed in OBS data from the North Atlantic - new seismic tool for oceanography? Polish Polar Research, 32, 405-422.F doi: https://doi.org/10.2478/v10183-011-0027-3.

Grimstad, S., 2016. Salt tectonics in the central and northeastern Nordkapp Basin, Barents Sea. Master thesis, Dept. of Geol., Univ. of Oslo, Oslo, Norway.

Grogan, P., Østvedt-Ghazi, A.M., Larssen, G.B., Fotland, B., Nyberg, K., Dahlgren, S., Eidvin, T., 1999. Structural elements and petroleum geology of the Norwegian sector of the northern Barents Sea. In: Fleet, A.J., Boldy, S.A.R. (Eds.), Petroleum Geology of the Northwest Europe: Proceedings of the 5th Conference. Geological Society, London, pp. 247-259 doi: doi: 10.1144/0050247.

Grogan, P., Nyberg, K., Fotland, B., Myklebust, R., Dahlgren, S., Riis, F., 2000. Cretaceous magmatism south and east of Svalbard: evidence from seismic reflection and magnetic data. Polarforschung 68, 25-34.

Gudlaugsson, S.T., Faleide, J.I., Fanavoll, S., Johansen, B., 1987. Deep seismic reflection profiles across the western Barents Sea. Geophys. J. R. Astron. Soc., 89, 273-278 doi: https://doi.org/10.1111/j.1365-246X.1987.tb04419.x.

Gudlaugsson, S.T., Faleide, J.I., Johansen, S.E, Breivik, A.J., 1998. Late Palaeozoic structural development of the South-western Barents Sea. Marine and Petroleum Geology 15, 73-102 doi: https://doi.org/10.1016/S0264-8172(97)00048-2.

Gudlaugsson, S.T., Faleide, J.I., 1994. The continental margin between Spitsbergen and Bjørnøya. In: Eiken, O. (Ed.), Seismic Atlas of Western Svalbard, Medd.-Nor. Polarinst., vol. 130, pp 11-13.

Harland, W.B., Anderson, L.M., Manasrah, D., 1997. The Geology of Svalbard. Memoir Geological Society of London 17, 521.

Harland, W. B., Gayer, R.A., 1972. The Arctic Caledonides and earlier oceans. Geological Magazine 109, 289-314 doi: https://doi.org/10.1017/S0016756800037717.

Henriksen, E., Ryseth, A.E., Larssen, G.B., Heide, T., Rønning, K., Sollid, K., Stoupakova, A.V., 2011a. Tectonostratigraphy of the greater Barents Sea: implications for petroleum systems. In: Spencer, A.M., Embry, A.F., Gautier, D.L., Stoupakova, A.V., Sørensen, K. (Eds.) Arctic Petroleum Geology. Memoirs Geological Society of London 35, 163-195 doi:10.1144/M35.10.

Henriksen, E., Bjørneseth, H.M., Hals, T.K., Heide, T., Kiryukhina, T., Kløvjan, O.S., Larssen, G.B., Ryseth, A.E., Rønning, K., Sollid, K., Stoupakova, A., 2011b. Uplift and erosion of the greater Barents Sea: impact on prospectivity and petroleum systems. In: Spencer, A.M., Embry, A.F., Gautier, D.L., Stoupakova, A.V., Sørensen, K. (Eds.) Arctic Petroleum Geology. Memoirs Geological Society of London 35, 271-281, doi: 10.1144/M35.17

Higgins, A.K., Leslie, A.G., 2000, Restoring thrusting in the East Greenland Caledonides. Geology 28, 1019-1022 doi: 10.1130/0091-7613(2000)28<1019:RTITEG>2.0.CO;2.

Jakobsson, M., Mayer L., Coakley B., Dowdeswell, J.A., Forbes, S., Fridman, B., Hodnesdal, H., Noormets, R., Pedersen, R., Rebesco, M., Schenke, H.W., Zarayskaya, Y., Accettella, D., Armstrong, A., Anderson, R.M., Bienhoff, P., Camerlenghi, A., Church, I., Edwards, M., Gardner J.V., Hall, J.K., Hell, B., Hestvik, O., Kristoffersen, Y., Marcussen, C., Mohammad, R., Mosher, D., Nghiem, S.V., Pedrosa, M.T., Travaglini, P.G., Weatherall, P., 2012. The International Bathymetric Chart of the Arctic Ocean (IBCAO) Version 3.0. Geophys. Res. Lett. 39 doi: 10.1029/2012GL052219.

Kenyon, S., Forsberg, R., Coakley, B., 2008. New gravity field for the Arctic. Eos Trans. AGU 89, 1-2 doi: 10.1029/2008EO320002.

Klitzke, P., Sippel, J., Faleide, J.I., Scheck-Wenderoth, M., 2016. A 3D gravity and thermal model for the Barents Sea and Kara Sea. Tectonophysics 684, 131-147 doi: http://dx.doi.org/10.1016/j.tecto.2016.04.033.

Krysinski, L., Grad, M., Mjelde, R., Czuba, W., Guterch, A., 2013. Seismic and density structure of the lithosphere-asthenosphere system along transect Knipovich Ridge-Spitsbergen-Barents Sea – geological and petrophysical implications. Polish Polar Research 34 (2), 111-138 doi: https://doi.org/10.2478/popore-2013-0011.

Leever, K.A.. Gabrielsen, R.H., Faleide, J.I., Braathen, A., 2001. A transpressional origin for the West Spitsbergen ford-and-thrust belt: Insight from analog modeling. Tectonics 30, TC2014, doi:10.1029/2010TC002753.

Levshin, A.L., Schweitzer, J., Weidle, C., Shapiro, N.M., Ritzwoller, M.H., 2007. Surface wave tomography of the Barents Sea and surrounding regions. Geophys. J. Int. 170, 441-459 doi: https://doi.org/10.1111/j.1365-246X.2006.03285.x.

Lorenz, H, Gee, D.G., Whitehouse, M.J., 2007. New geochronological data on Palaeozoic igneous activity and deformation in the Severnaya Zemlya Archipelago, Russia, and implications for the development of the Eurasian Arctic margin. Geological magazine 144, 105-125 doi: https://doi.org/10.1017/S001675680600272X.

Ludwig, W.I., Nafe, J.E, Drake, C.L., 1970. Seismic refraction. The Sea 4 (1), 53-84.

Marello, L., Ebbing, J., Gernigon, L., 2010. Magnetic basement study in the Barents Sea from inversion and forward modelling. Tectonophysics 493, 153-171 doi:10.1016/j.tecto.2010.07.014.

Marello, L., Ebbing J., Gernigon, L., 2013. Basement inhomegenities and crustal setting in the Barents Sea from a combined 3D gravity and magnetic model. Geophys. J. Int. 193, 557-584 doi: 10.1093/gji/ggt018.

Minakov, A., Mjelde, R., Faleide, J.I., Flueh, E.R., Dannowski, A., Keers, H., 2012. Mafic intrusions east of Svalbard imaged by active-source seismic tomography. Tectonophysics 518-521, 106-118 doi:10.1016/j.tecto.2011.11.015.

Minakov, A., Bretel, P., Lebedeva-Ivanova, N., Meyer, O., 2014. Cruise report: Barents OBS 2014, Ocean Bottom Survey In The Barents Sea, University of Oslo report, 35 pp.

Ohm, S.E., Karlsen, D.A, Austin, T.J.F., 2008. Geochemically driven exploration models in uplifted areas: Examples from the Norwegian Barents Sea. AAPG Bulletin 92 (9), 1191-1223 doi: 10.1306/06180808028.

Olovyanishnikov, V.G., Siedlecka, A., Roberts, D., 1997. Aspects of Geology of the Timans, Russia and linkage with Varanger Peninsula, NE Norway. Bulletin of the Geological Survey of Norway 433, 28-29.

Polteau, S., Hendriks, B.W.H., Planke, S., Ganerød, M., Corfu, F., Faleide, J.I., Midtkandal, I., Svensen, H.S., Myklebust, R., 2016. The Early Cretaceous Barents Sea Sill Complex: Distribution, $^{40}Ar/^{39}Ar$ geochronology, and implications for carbon gas formation. Palaeogeography, Palaeoclimatology, Palaeoecology 441, 83-95 doi: http://dx.doi.org/10.1016/j.palaeo.2015.07.007.

Ritzmann, O., Faleide, J.I., 2007. Caledonian basement of the western Barents Sea. Tectonics 26 (5), 1-20 doi:10.1029/2006TC002059 TC5014.

Roberts, D., Gee, D.G., 1985. An introduction to the structure of the Scandinavian Caledonides. In: Gee, D.G., Sturt, B.A. (Eds.) The Caledonide Orogen – Scandinavia and Related Areas. John Wiley & Sons, Chichester 55-68.

Roberts, D., Siedlecka, A., 2002. Timanian orogenic deformation along the northeastern margin of Baltica, Northwest Russia and Northeast Norway, and Avalonia-Cadomian connections. Tectonophysics 352 (1-2), 169-184 doi: http://dx.doi.org/10.1016/S0040-1951(02)00195-6.

Roberts, D., Olovyanishnikov, V., 2004. Structural and tectonic development of the Timanide orogen. In: Gee, D.G., Pease, V. (Eds.) The Neoproterozoic Timanide Orogen of Eastern Baltica. Memoirs Geological Society of London 30, 47-57 doi: 10.1144/GSL.MEM.2004.030.01.05.

Smelror, M., Petrov, O., Larsen, G.B., Werner, S.C., 2009, Atlas: Geological History of the Barents Sea. Geological Survey of Norway, Trondheim.

Torsvik, T.H., Van der Voo, R., Meert, J.G., Mosar, J., Walderhaug, H.J., 2001. Reconstructions of the continents around the North Atlantic at about the 60th parallel. Earth Planet. Sci. Lett. 187, 55-69 doi:

http://dx.doi.org/10.1016/S0012-821X(01)00284-9

Wessel, P., Smith, W.H.F., 1998. New, improved version of Generic Mapping Tools released. EOS Trans. Am. Geophys. U. 79, 579 doi: 10.1029/98EO00426.

Zelt, C.A., Forsyth, D.A., 1994. Modeling wide-angle seismic data for crustal structure: southeastern Grenville Province. J. Geophys. Res. 99 (B6), 11687-11704 doi: 10.1029/93JB02764.

Zelt, C.A., Smith, R.B., 1992. Seismic traveltime inversion from 2-D crustal velocity structure. Geophys. J. Int. 108, 16-34 doi: https://doi.org/10.1111/j.1365-246X.1992.tb00836.x.

Ziegler, P.A., 1988. Evolution of the Arctic-North Atlantic and the Western Tethys. AAPG Memoirs, Tulsa 43, 1-198.

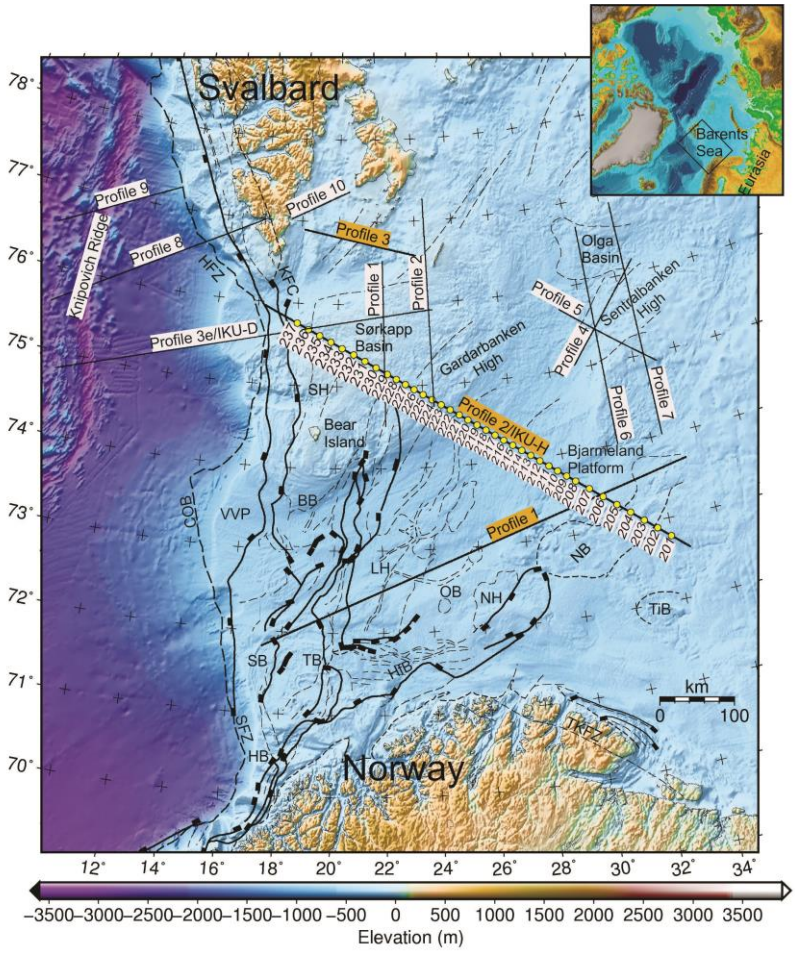

Fig.1: Location the modeled profile 2 with OBS locations marked by yellow dots. Profiles 1 and 3 are also shown. Bathymetry is taken from Jakobsson et al. (2012) fault positions from Faleide et al. (1993), outline of basin and highs from Gabrielsen et al. (1990). COB: continent-ocean boundary from Breivik et al. (1999) BB: Bjørnøya Basin, HB: Harstad Basin, HfB: Hammerfest Basin, HFZ: Hornsund Fault Zone, KFC: Knølegga Fault Complex, LH: Loppa High, NB: Nordkapp Basin, NH: Norsel High, OB: Ottar Basin, SB: Sørvestsnaget Basin, SH: Stappen High, TB: Tromsø Basin, TiB: Tiddlybanken Basin, TKFZ: Trollfjorden-Komagelva Fault Zone, VVP: Vestbakken Volcanic Province.

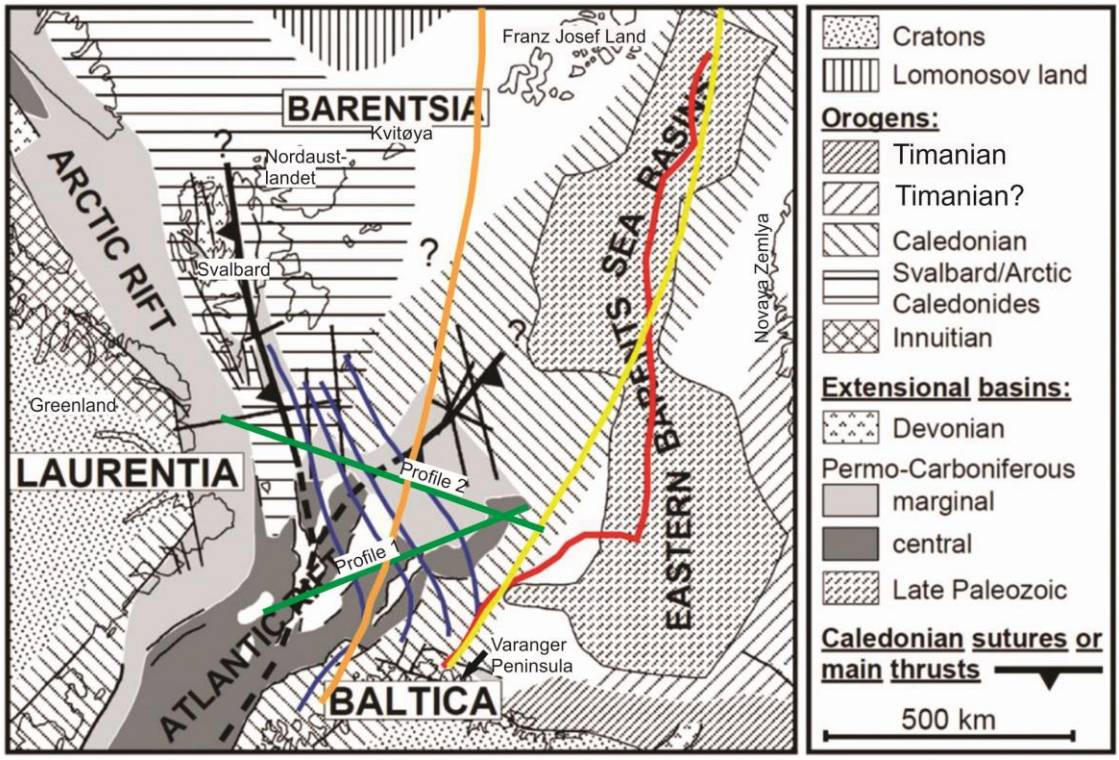

Fig. 2: Caledonide model of Gudlaugsson et al. (1998) compared with different interpretations of Caledonian structural trends. Black: OBS profiles modeled by Breivik et al. (2002, 2003 and 2005) and proposed Caledonian suture zones (Breivik et al., 2005). Orange: Proposed Caledonian suture (Gee at al., 2006). Yellow: Proposed Caledonian deformation front (Gee at al., 2006). Red: Proposed Caledonian deformation front (Henriksen et al., 2011). Blue: Prolongation of Caledonian thrusts (Barrère et al., 2009; Gernigon and Brönner, 2012; Gernigon et al., 2014). Green: OBS profiles 1 and 2 from this study. In the original figure Timanian was referred to as Baikalian.

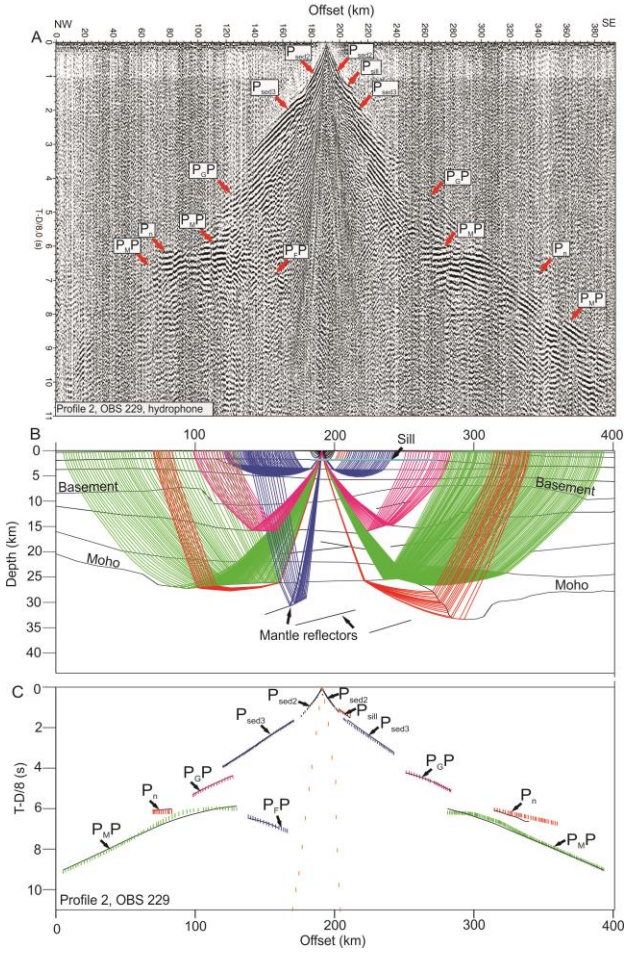

Fig.3. A: Seismic data from OBS 229, profile 2, hydrophone component *(BP-filter (4-16 Hz), spiking decon. and AGC applied).* Phase codes are listed in Table 1. B: Ray-paths through velocity layer model for OBS 229. C: Interpreted (vertical bars) and calculated travel-time curves.

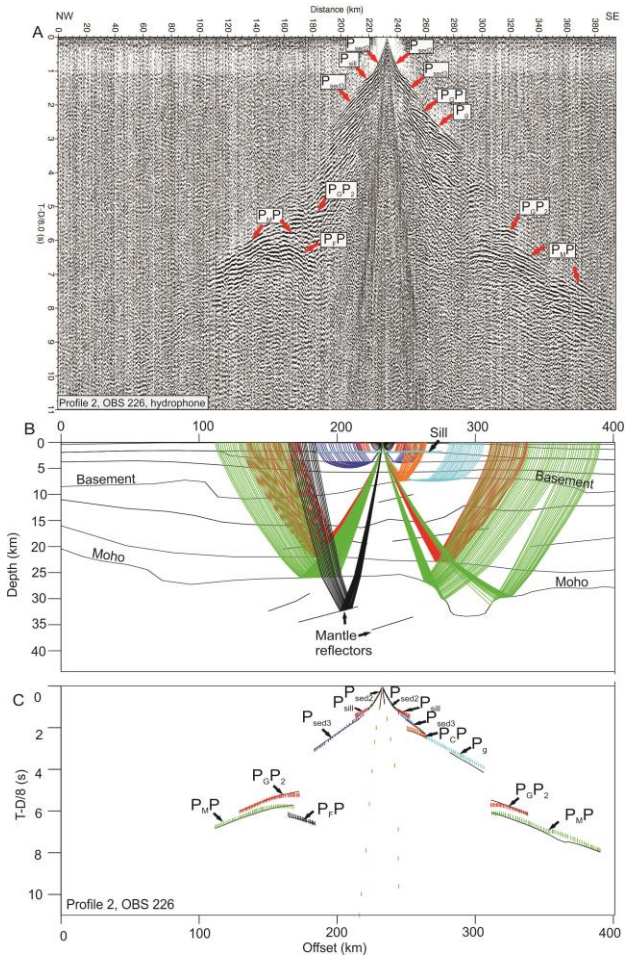

Fig.4. A: Seismic data from OBS 226, profile 2, hydrophone component *(BP-filter (4-16 Hz), spiking decon. and AGC applied).* Phase codes are listed in Table 1. B: Ray-paths through velocity layer model for OBS 226. C: Interpreted (vertical bars) and calculated travel-time curves.

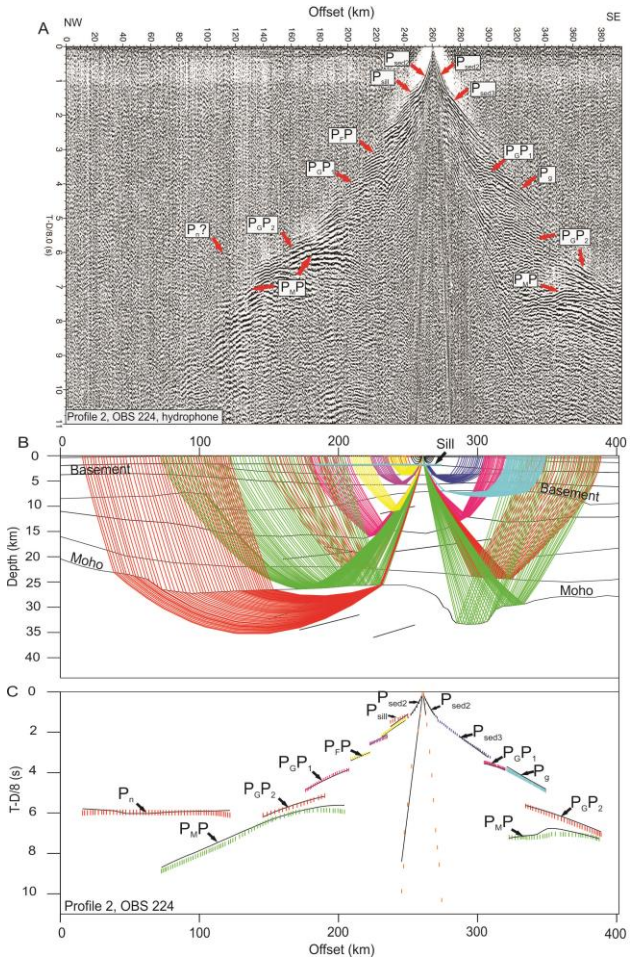

Fig.5. A: Seismic data from OBS 224, profile 2, hydrophone component *(BP-filter (4-16 Hz), spiking decon. and AGC applied).* Phase codes are listed in Table 1. B: Ray-paths through velocity layer model for OBS 224. C: Interpreted (vertical bars) and calculated travel-time curves.

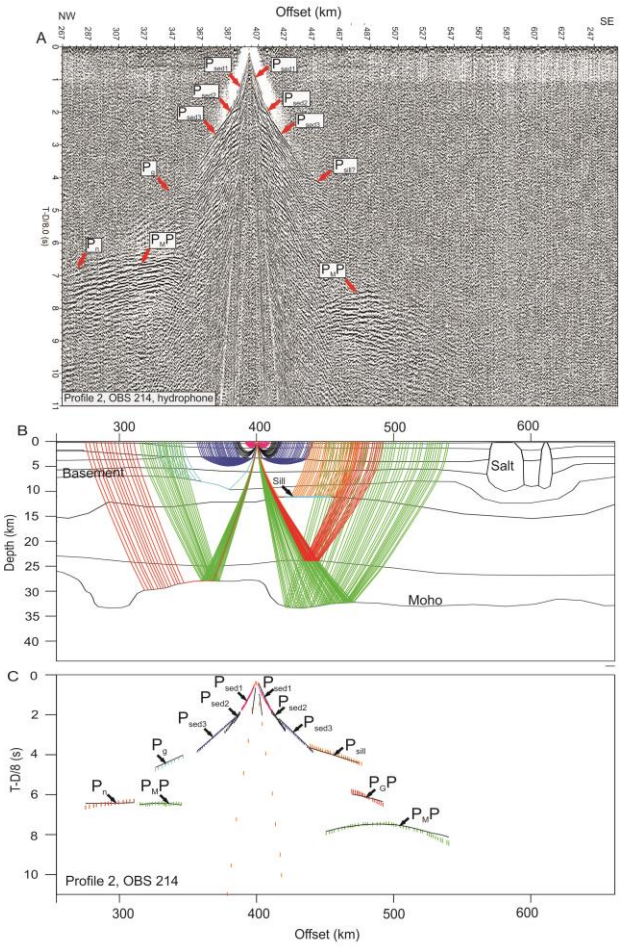

Fig.6. A: Seismic data from OBS 214, profile 2, hydrophone component *(BP-filter (4-16 Hz), spiking decon. and AGC applied).* Phase codes are listed in Table 1. B: Ray-paths through velocity layer model for OBS 214. C: Interpreted (vertical bars) and calculated travel-time curves.

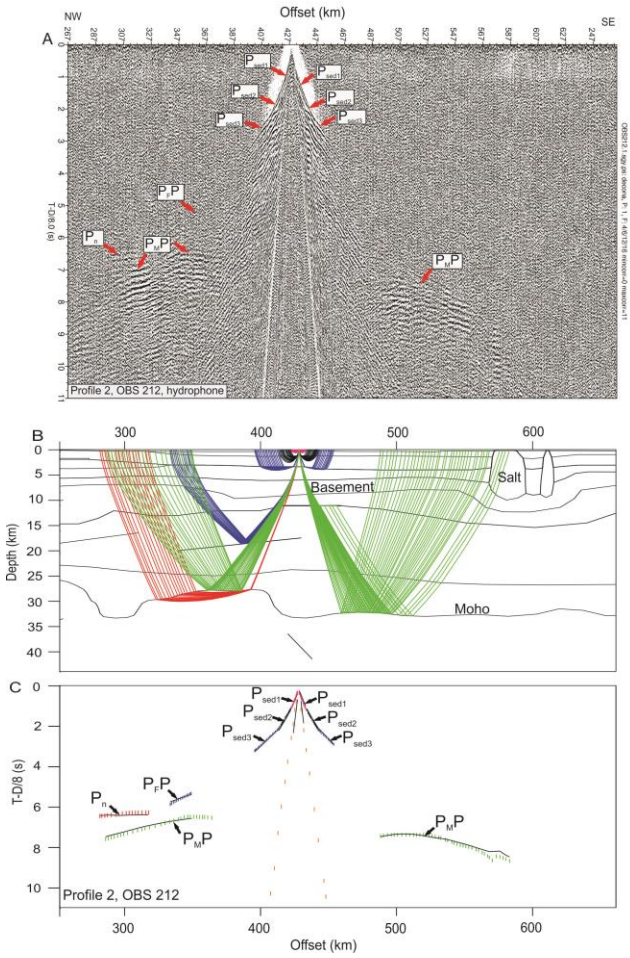

Fig.7 A: Seismic data from OBS 212, profile 2, hydrophone component *(BP-filter (4-16 Hz), spiking decon. and AGC applied)*. Phase codes are listed in Table 1. B: Ray-paths through velocity layer model for OBS 212 C: Interpreted (vertical bars) and calculated travel-time curves.

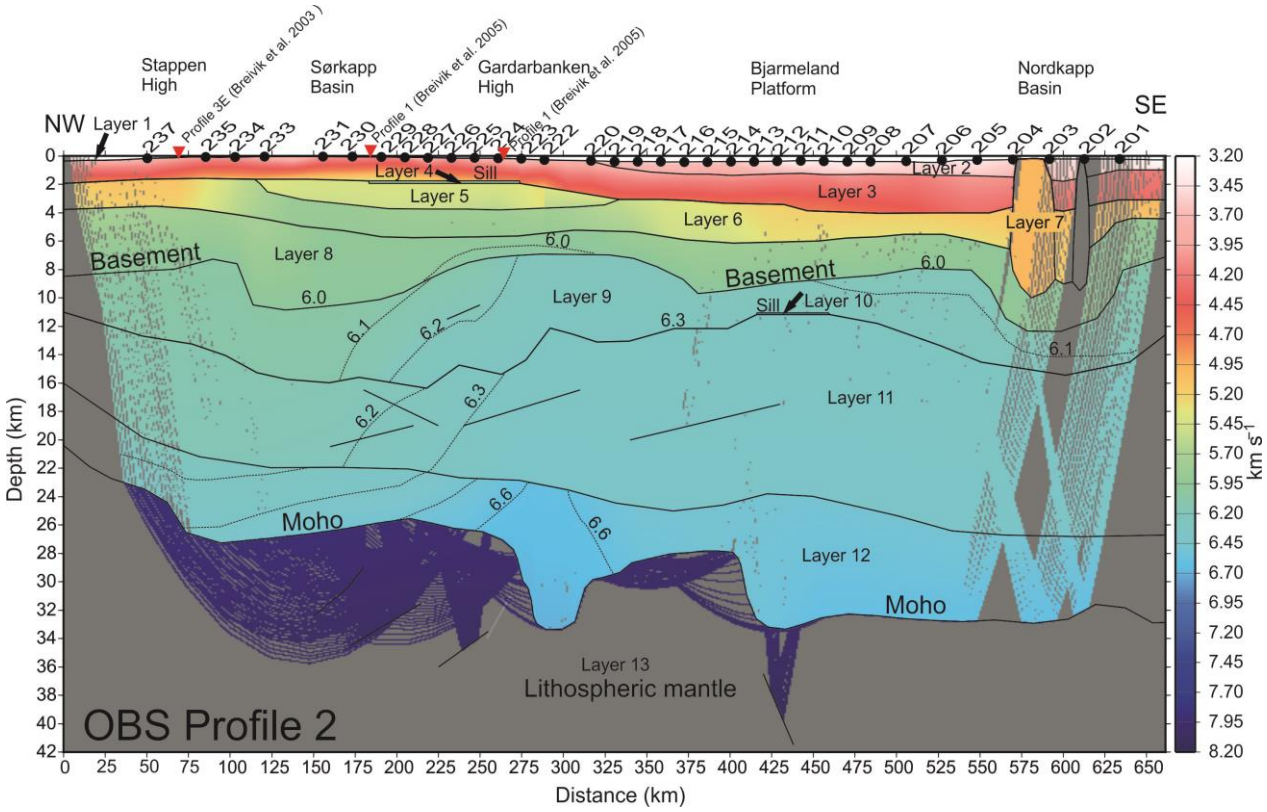

Fig. 8: P-wave velocity model of profile 2 with layers numbered 1-13. Velocities from 6.0 to 6.6 km/s are contoured and annotated. Grey areas are not covered by ray-paths and are unconstrained. The location of crossing profiles is indicated by red triangles.

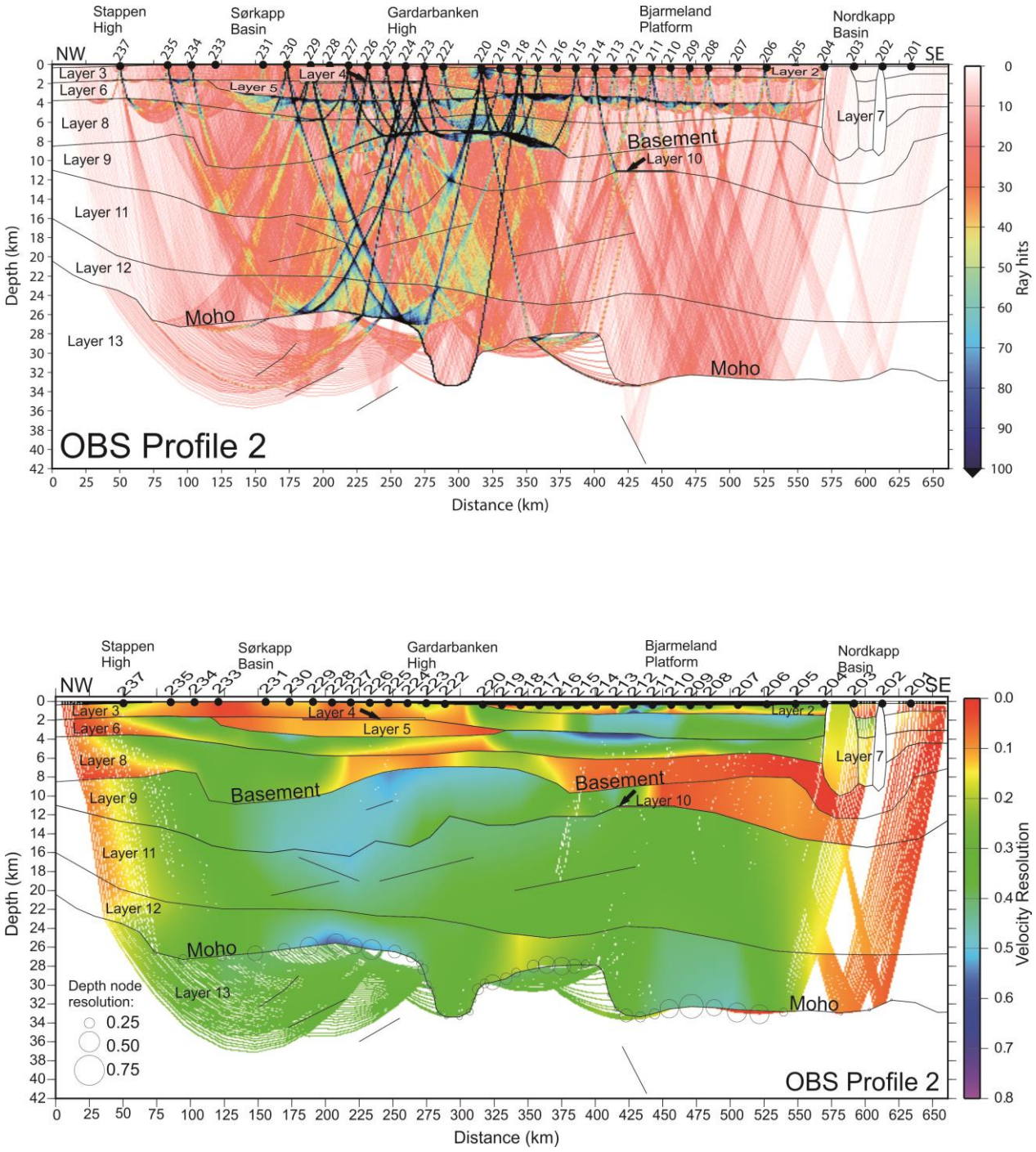

Fig. 9 A: Gridded ray coverage of the velocity model. The binning is 2.5 km horizontally and 0.25 km with depth. B: Resolution parameters of the velocity model. The velocity node resolution is shown by the color scale while the Moho depth resolution is given by the size of the circles, the larger the better constrained.

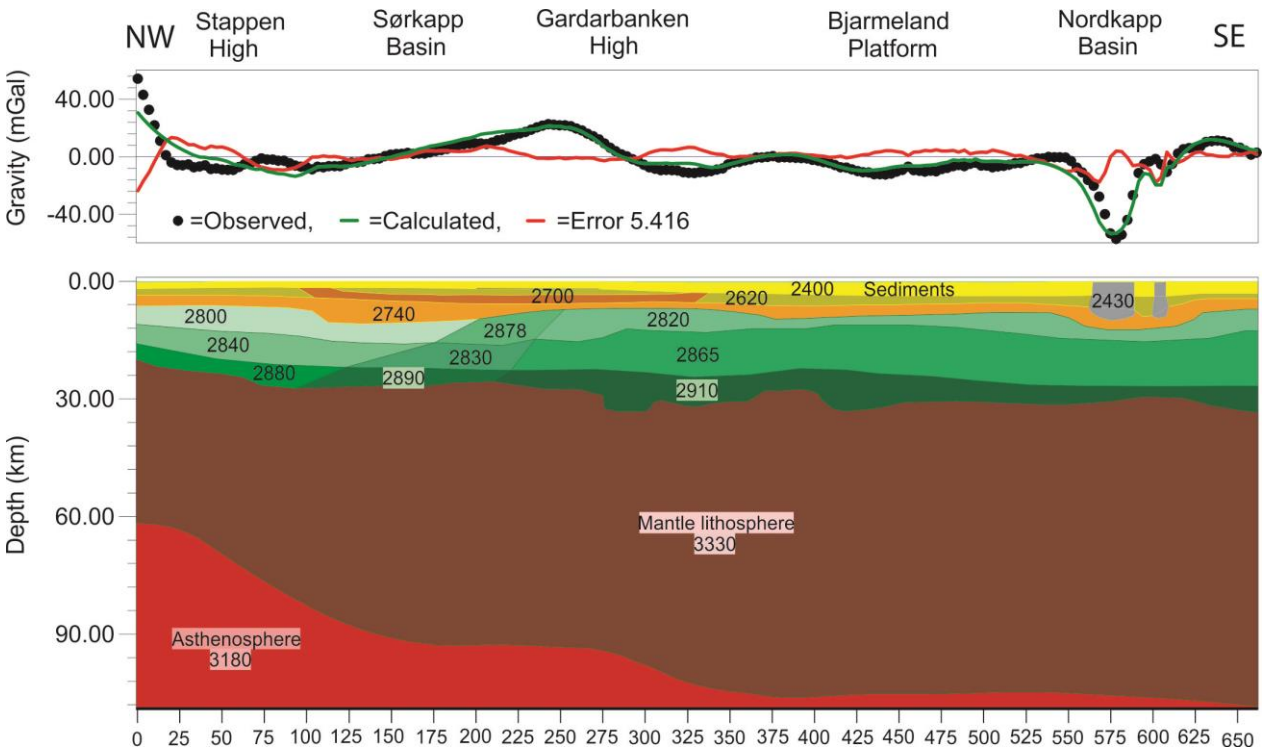

Fig. 10: Gravity model along Profile 2. Numbers on figure are densities in kg/m^3. Sediments are shown in yellow and basement blocks in green.

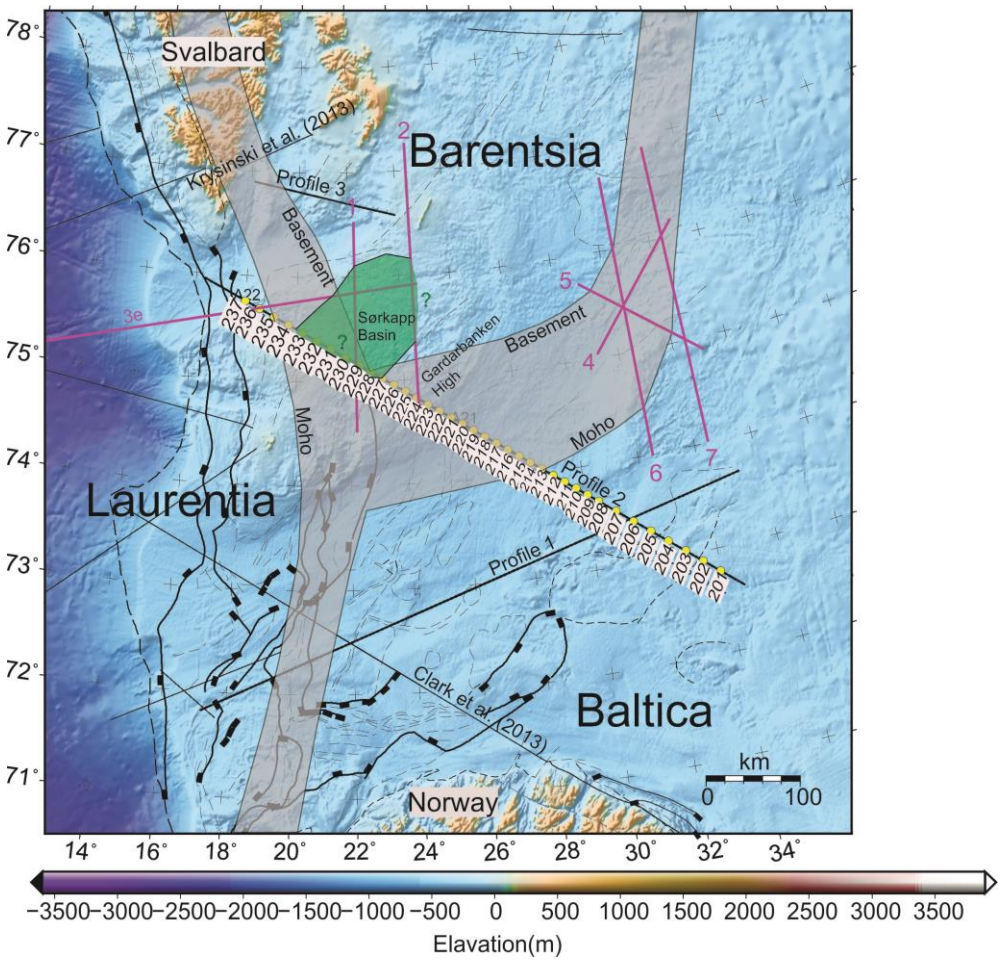

Fig.11: Location of the modeled profile with OBS locations shown as yellow dots. The shaded gray area indicates the location of the proposed Caledonian suture zones. The map is based on a Caledonide model of Gudlaugsson et al. (1998), OBS profiles (in pink) modeled by Breivik et al. (2002, 2003, 2005), Clark et al. (2013) and Krysinski et al. (2013). The edges of the gray area is where the suture zone cuts top basement and Moho. The sørkapp Basin is outlined in green.

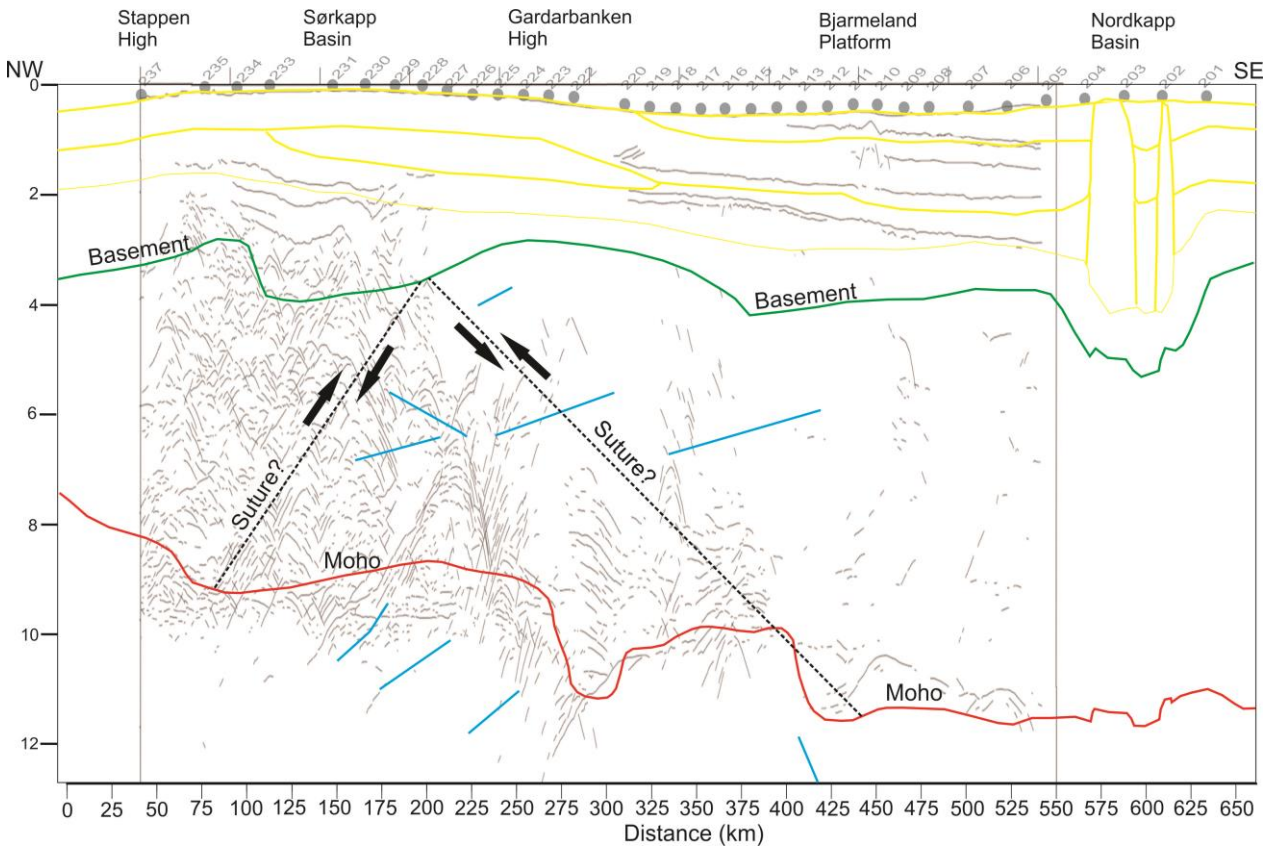

Fig.12: Velocity model from OBS data compared to linedrawing of the MCS line IKU-H. Coloured and stippled lines are from the OBS data, floating reflectors are indicated in blue. The proposed Caledonian suture from Figs. 12 and 13 separates the reflective basement in the west from the more transperant basement in the east. Modified from Gudlaugsson et al. (1987) and Ritzmann and Faleide (2007).

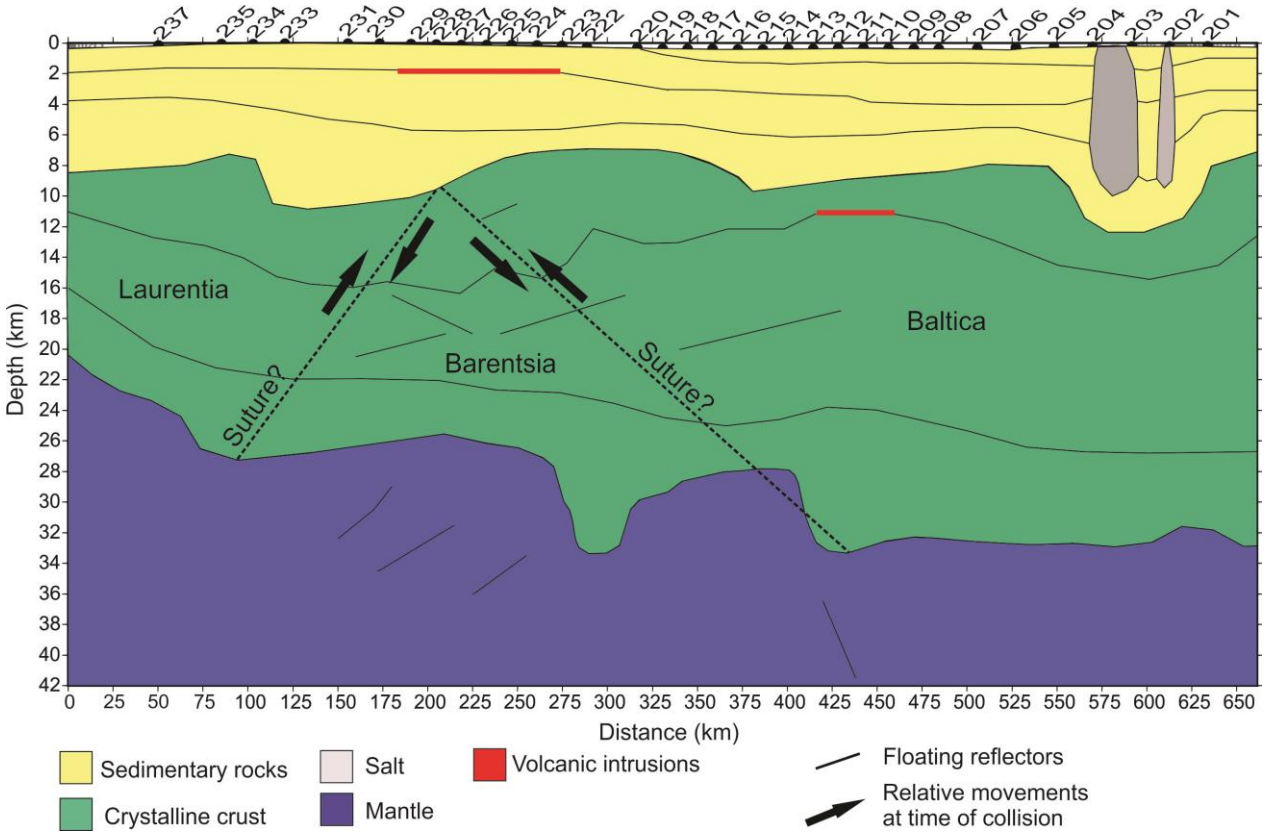

Fig.13: Tectonic model of the modeled OBS profile.

Table 1: List of abbreviations used for seismic events

Phase	**Code**
P-wave refraction from sedimentary section 1	P_{sed1}
P-wave refraction from sedimentary section 2	P_{sed2}
P-wave refraction from sedimentary section 3	P_{sed3}
P-wave refraction at igneous sills	P_{sill}
P-wave refraction top basement	P_g
P-wave reflection top basement	P_CP
P-wave reflection from within crystalline crust 1	P_GP_1
P-wave reflection from within crystalline crust 2	P_GP_2
P-wave refraction from top mantle	P_n
P-wave reflection from Moho	P_MP
P-wave reflection from floating reflectors	P_FP

Table 2: Velocity model statistics for major refracted and reflected phases. P_GP_1 and P_GP_2 ere reflections from upper and lower crustal layers. Total values include reflections that have not been listed .

Phase	Number of picks	T_{RMS} (ms)	Normalized Chi-Squared
$\mathbf{P_{sed1}}$	337	111	1.988
$\mathbf{P_{sed2}}$	656	72	1.332
$\mathbf{P_{sed3}}$	1173	62	0.878
$\mathbf{P_{sill}}$	63	87	1.565
$\mathbf{P_g}$	343	94	1.165
$\mathbf{P_CP}$	62	112	1.425
$\mathbf{P_GP_1}$	181	65	0.597
$\mathbf{P_GP_2}$	214	83	0.770
$\mathbf{P_n}$	343	94	1.165
$\mathbf{P_MP}$	1613	128	1.598
Total	5470	97	1.231

Table 3: Profile 2 compared with three crossing seismic profiles. Velocities and densities listed are at the top and bottom of the given unit. The location of crossing profiles is shown on Figs. 1, 8 and 11.

	Crosspoint 1		**Crosspoint 2**		**Crosspoint 3**	
	Laurentia		Barentsia		Barentsia/Baltica	
	P3e	**OBS 236**	**P1**	**OBS 229**	**P2**	**OBS 224**
Sedimentary unit: Vp (km/s)	4.0-6.0	4.0-6.0	4.0-6.0	4.0-6.0	4.0-6.0	4.0-6.0
Sedimentary unit: δ (g/cm3)	2.46-2.69	2.40-2.75	2.40-2.75	2.40-2.75	2.40-2.75	2.40-2.75
Crystalline crust: Vp (km/s)	6.2-6.4	6.05-6.4	6.2-6.6	6.1-6.5	6.2-6.6	6.2-6.6
Crystalline crust: δ (g/cm3)	2.798	2.78-2.87	2.797	2.82-92	2.818	2.82-92